2018 International Conference on Indoor Positioning and Indoor Navigation (IPIN), 24-27 September 2018, Nantes, France

QADA-plus: a novel two-stage receiver for visible light positioning

Stefanie Cincotta, Cuiwei He, Adrian Neild and Jean Armstrong
Monash University
Melbourne, Australia
{Stefanie.Cincotta, Cuiwei.He, Adrian.Neild, Jean.Armstrong}@monash.edu

***Abstract*— In this paper, we introduce a new two-stage receiver structure for visible light positioning (VLP) and a particular implementation of the new structure called the QADA-plus receiver. By using two sensors, one a photodiode (PD) based sensor and the other an image-based sensor, the new structure exploits the strengths of both technologies while avoiding their weaknesses. The QADA-plus uses a quadrant angular diversity aperture receiver (QADA) for the PD-based stage. The QADA has a very compact, planar structure suitable for incorporation in a smartphone or other small device and has been shown to provide good angular diversity in a proof-of-concept laboratory experiment. The QADA is also, unlike typical image sensors, able to reliably demodulate high frequency visible light signals. In this paper extensive simulation results for a range of typical indoor scenarios and realistic parameters show that the QADA has the potential to accurately estimate the polar and incident angle of light transmitted by LED luminaires. The average absolute error in estimation of incident angle was 0.0006° and for polar angle estimation was 0.005°. A limitation of these simulations is that it is assumed that the luminaires can be modelled as point sources and that the dimensions of the QADA are very precisely known. Incorporation of the QADA in the new two-stage QADA-plus receiver removes these limitations in two ways – the image-based receiver provides very accurate angle-of-arrival estimates and the use of visible reference points means that the QADA-plus is compatible with luminaires of any shape.**

Keywords—visible light positioning, quadrant photodiode, aperture, QADA, QADA-plus

I. INTRODUCTION

Recently, because of the widespread introduction of LED based indoor lighting, there has been significant and increasing interest in the use of visible light communications (VLC) for indoor positioning [1], [2]. Unlike conventional lighting, LEDs can be modulated at high rates. Receivers, using photodiodes (PDs) or imaging sensors, detect the signals and determine the receiver position. A major advantage of visible light positioning (VLP) is that it takes advantage of existing lighting infrastructure and so reduces the cost of installation dramatically [1]. Additionally, unlike radio frequency (RF) based methods, it is not subject to significant multipath propagation issues [3].

There are many different approaches to VLP each with their own strengths and weaknesses. One of the most intuitive approaches is to use the received signal strength (RSS) to determine the distance from the transmitter to the receiver [4]–[6]. However, without very accurate knowledge of the transmitted power and the optical channel, it is difficult to accurately estimate this distance. Alternative well-known methods use time-of-arrival (TOA) or time-difference-of-arrival (TDOA) [7], [8]. Whilst the latter works well for GPS, it is not practical for VLP due to the expensive synchronized clocks that are required and the very small time differences that would need to be accurately measured.

Another alternative is to estimate the angle-of-arrival (AOA) of the received light. This is possible because there is typically a line-of-sight (LOS) path available from the LED beacons to the receiver. AOA estimation requires an angular diversity optical receiver. This can be implemented using either imaging sensors [9]–[11] or PDs [12]–[15]. Imaging sensors generally have high resolutions making them well suited to accurate AOA estimation, but because of frame rate limitations, they are not able to demodulate high-frequency signals. This is a major limitation because to avoid adverse biological effects [16], modulation of LEDs at low frequencies must be avoided. A number of innovative workarounds have been proposed which depend on the rolling shutter mechanism of typical low cost digital cameras [17] but these systems can only provide rough positioning and can demodulate only relatively low data rate signals.

In the past, a number of PD-based receivers have achieved angular diversity by having PDs facing in different directions [13], [15]. These three-dimensional PD structures have been shown to provide good angular diversity, however, they are not well suited to integration into modern consumer electronics due to the awkward protrusion they create. The quadrant angular diversity aperture (QADA) receiver solves this problem by combining an aperture with a quadrant PD [18], [19]. We have previously demonstrated that this achieves good angular diversity within a compact and planar structure.

In this paper, we present a completely new approach and describe an all-new hybrid two-stage receiver, called QADA-plus. The new receiver has two distinct sensors: one a PD-based sensor and the other an imaging sensor. In this way, we build on the strengths and avoid the weaknesses of each type of sensor. In the system described in this paper, the first stage uses the QADA receiver to demodulate the signals and identify the LED beacons. The second stage captures a still image and combines this with the information from the first stage to

This work was supported by the Australian Research Council's (ARC) Discovery funding schemes (DP150100003 and DP180100872) and an Australian Government Research Training Program (RTP) Scholarship.

978-1-5386-5635-8/18/$31.00 ©2018 Crown

achieve accurate positioning. We also describe how, by associating precise visible reference points with each luminaire, the performance can be further improved.

The significant contributions of this paper include

1. The first publication of the all new two-stage positioning receiver that provides high accuracy.
2. The use of reference point or points to identify precise position(s) associated with each luminaire[1].
3. A detailed analysis of QADA in two dimensions, including angular diversity analysis

Section II provides a detailed description of each of the two stages of the system and the use of reference points. In Section III the results of simulations are presented that demonstrate the suitability of the QADA receiver for stage one. Section IV is a discussion on realistic implementations and Section VI contains the conclusions.

II. System Description

Fig. 1 shows the overall structure of a positioning system using the new QADA-plus two-stage receiver. Each LED beacon transmits an optical signal which contains information about its position. In this paper, we call the position information message transmitted by the n^{th} LED beacon the Beacon Information packet (BIP_n). The BIP message contains information about the positions of the reference point, or points, on the luminaire. Reference points are specific points on the luminaire that can be identified by an image sensor. We discuss the use of reference points in detail in a later section.

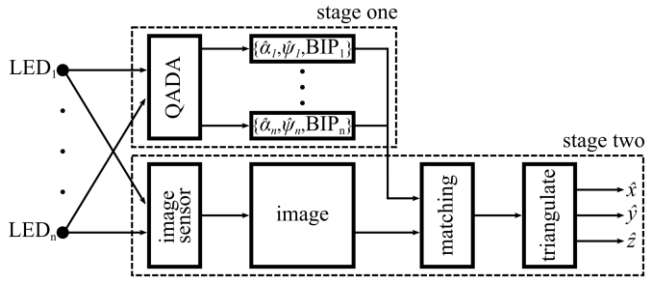

Fig. 1. Block diagram showing the overall structure of the receiver and the flow of information between stage one and stage two.

Light from each transmitter is received by both the PD-based sensor and the image sensor. The PD-based sensor, which in this paper is a QADA, demodulates the signals transmitted by each LED beacon and decodes the BIP messages for all of the transmitters within range. We assume that the LED beacons transmit orthogonal signals so that the signals from each can be readily separated at the receiver. For example, time-division-multiplexed or frequency-division-multiplexed signals could be used. The PD-based sensor simultaneously provides approximate estimates of the incident angle, ψ, and the polar angle, α, of all LED beacons in the field-of-view (FOV). At the same time, the image-based sensor takes a high-resolution image that includes the luminaires. The outputs of the two sensors are then used in the matching stage. The approximate incident angle and polar angle of the LED beacon from the first stage allows each luminaire to be unambiguously identified in the image. This, in combination with the position information contained in the BIP message, allows the precise positions of the reference points in the image plane to be very accurately determined. By using the AOA information from three or more reference points, well-known triangulation algorithms can be used to calculate the x, y, and z coordinates of the receiver. This method is more accurate than using a single-stage QADA receiver.

A. Stage one – QADA

The QADA receiver, in Fig. 2, consists of a quadrant PD, shown in blue, positioned directly below a transparent aperture. A quadrant PD is a type of segmented PD that consists of four discrete PDs arranged in a 2 x 2 array. The PDs are separated by a very narrow gap. Segmented PDs are available in varying shapes, sizes and number of segments and are typically used in laser light applications such as beam centering [20], [21] where they are capable of providing position information in two dimensions. In these applications, an aperture is not required. The combination of an aperture with a quadrant PD in the form of the QADA and its potential in indoor positioning applications has only been very recently described [18].

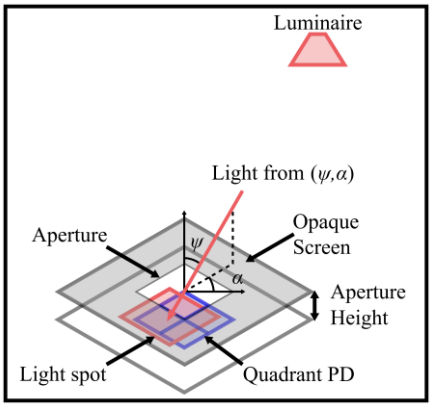

Fig. 2. QADA receiver structure.

The aperture plane is separated from the quadrant PD plane by a known vertical distance, h. We call this distance the aperture height. In Fig. 2, the light from an LED luminaire passes through the aperture and forms a light spot, shown in red, on the quadrant PD. The light spot shape and size match that of the aperture. The position of this light spot is unique for a given AOA provided that the aperture is no larger than the quadrant PD and the dimensions of the light beacon are much smaller than the distance from the beacon to the receiver.

We use a square aperture and quadrant PD so that the position of the light spot maintains a linear relationship as it passes over the quadrant PD [18]. We choose an aperture size that matches the quadrant PD size as we have previously shown that this maximizes the signal-to-noise ratio (SNR) for positioning [18].

[1] We use the term 'luminaire' as it is the technical term for the light fitting. Luminaires can be made up of one, or multiple, LEDs, of which some, or all, will be transmitting signals. We refer to the LEDs that are transmitting signals as the LED beacons.

First, we analyze how the position information for one beacon is determined, and then we will show how the use of orthogonal signals allows simultaneous calculation of the positions of multiple beacons.

The ratio of photocurrents in adjacent quadrant pairs is used to determine the position of the light spot centroid. In Fig. 3, the light spot, shown in yellow, overlaps the quadrant PD. The colors in the overlap areas represent the quadrant pairs used in the ratio function. In Fig. 3 (a), we determine the x coordinate of the centroid of the spot by using the ratios between the left and right quadrant pairs and in Fig. 3 (b), we determine the y coordinate of the centroid by using the ratios between the top and bottom quadrant pairs. The x and y coordinates of the centroid are estimated independently and then used, in combination with the known aperture height, to estimate the incident and polar angles of the incoming light.

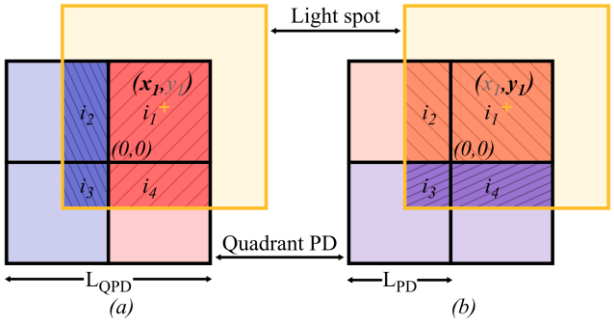

Fig. 3. Light spot overlapping the quadrant PD

These ratios are expressed as

$$p_x(t)=\frac{i_1(t)+i_4(t)+N_1(t)+N_4(t)}{i_2(t)+i_3(t)+N_2(t)+N_3(t)} \quad (1)$$

$$p_y(t)=\frac{i_1(t)+i_2(t)+N_1(t)+N_2(t)}{i_3(t)+i_4(t)+N_3(t)+N_4(t)} \quad (2)$$

where $i_j(t)$ and $N_j(t)$ are the photocurrent and noise generated by the j^{th} quadrant of the PD.

The LEDs are assumed to have a radiation pattern that is Lambertian with an order of $m=1$. The general expression for the channel gain for the j^{th} quadrant at time, t, is given by [22]

$$h_j(t)=\frac{(m+1)A_j(t)}{2\pi d^2(t)}\cos^m(\phi(t))T_s(\psi(t))g(\psi(t))\cos(\psi(t)) \quad (3)$$

where d is the distance between the transmitter and the receiver, ϕ is the emergence angle, ψ is the incidence angle, $A_j(t)$ is the area of quadrant j which the light spot overlaps, $T_s(\psi(t))$ is the filter transmission and $g(\psi(t))$ is the concentrator gain. As the QADA does not use any optical filters[2], lenses, or concentrators, the values of these parameters are set to 1, and thus, the photocurrent for the j^{th} quadrant at time, t, is given by

$$i_j(t)=\frac{RP_T A_j(t)\cos^2(\psi(t))}{\pi d^2(t)} \quad (4)$$

where R is the responsivity of the PD and P_T is the transmitted optical power.

From (4), it is clear that the photocurrent is directly proportional to the area of overlap. If we exclude the noise terms from the above functions, we can simplify them to a function of the overlap area. We define L_{PD} as the length of a single quadrant, shown in Fig. 3 (b), and $[x_1(t),y_1(t)]$ as the centroid of the light spot at time, t.Thus, in the absence of noise, the ratios in (1) and (2), can be expressed as:

$$p_x(t)=\frac{A_1(t)+A_4(t)}{A_2(t)+A_3(t)}=\begin{cases}\dfrac{L_{PD}+x_1(t)}{L_{PD}}, & -L_{PD}<x_1(t)\le 0\\ \dfrac{L_{PD}}{L_{PD}-x_1(t)}, & 0<x_1(t)<L_{PD}\end{cases} \quad (5)$$

$$p_y(t)=\frac{A_1(t)+A_2(t)}{A_3(t)+A_4(t)}=\begin{cases}\dfrac{L_{PD}+y_1(t)}{L_{PD}}, & -L_{PD}<y_1(t)\le 0\\ \dfrac{L_{PD}}{L_{PD}-y_1(t)}, & 0<y_1(t)<L_{PD}\end{cases} \quad (6)$$

We can now rearrange (5) and use the result to derive an estimate for $x_1(t)$. The received signal undergoes low pass filtering to limit the bandwidth to B hertz, before sampling at the Nyquist rate, $2B$, and matched filtering to select the desired signal and reject any orthogonal signals received from other beacons [23]. We then average over M values to find the estimate at time $t=(k+M)/2B$, which can be expressed as

$$\hat{x}_1\left[\frac{k+M}{2B}\right]=\begin{cases}\dfrac{1}{M}\displaystyle\sum_{n=k}^{k+M-1}L_{PD}\left(p_x\left[\frac{n}{2B}\right]-1\right), & -L_{PD}<x_1\left[\dfrac{k+M}{2B}\right]\le 0\\ \dfrac{1}{M}\displaystyle\sum_{n=k}^{k+M-1}L_{PD}-\dfrac{L_{PD}}{p_x\left[\dfrac{n}{2B}\right]}, & 0<x_1\left[\dfrac{k+M}{2B}\right]<L_{PD}\end{cases} \quad (7)$$

The block diagram of this process is shown in Fig. 4

We can derive a similar estimate for $y_1(t)$. As can be seen in (7), the estimate for $x_1(t)$ depends only on the value of L_{PD} and p_x. It does not depend on the value of $y_1(t)$. However,

[2] Optical filters operate in the optical domain before the PD and are used to selectively transmit different wavelengths of light, whilst electrical filters operate in the electrical domain after the PD and remove unwanted electrical frequencies.

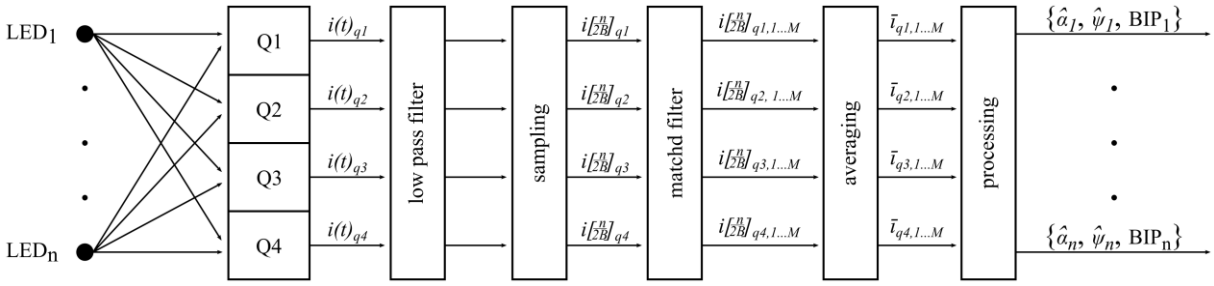

Fig. 4 Digital signal processing path for QADA

the photocurrent, $i_j(t)$, depends on the values of $x_1(t)$ and $y_1(t)$. Thus, the SNR is reduced because of the reduced area of overlap.

The noise in optical receivers is typically a combination of both the shot noise and the thermal noise [22]. The shot noise due to background illumination is the dominant noise source. It is modeled as a white Gaussian process. The variance of the shot noise for an isotropic receiver, expressed in (8), is the product of the single-sided noise power density and the electrical bandwidth, B.

$$\sigma_{\text{shot}}^2 = 2qRp_{\text{n}} A\Delta\lambda B \tag{8}$$

where q is the charge of an electron, p_{n} is the spectral irradiance, A is the area of the PD quadrant and $\Delta\lambda$ is the optical bandwidth.

The thermal noise is calculated using the noise equivalent power (NEP). Like the shot noise, it is the product of the spectral density and the electrical bandwidth.

$$\sigma_{\text{thermal}}^2 = \left(NEP \times R\right)^2 B \tag{9}$$

QADA is a well suited AOA detector for stage one. Using a small 5 mm square quadrant PD, its compact planar structure means that it can be easily incorporated into a smartphone and it provides sufficiently accurate AOA data for input to stage two.

B. *Stage two – Image sensor*

Image sensors, such as cameras typically found in smartphones, can provide very high angular resolution as they typically have a large number of pixels. Position accuracy in the sub-decimeter range has been shown to be possible using high megapixel cameras [11], [24], [25]. However, demodulation of transmitted data is difficult without high frame rates or complex algorithms [26]–[28]. In QADA-plus, this is avoided by using a PD-based AOA detector to demodulate the signals and identify the LED beacons. This information from stage one, consisting of an AOA estimate and BIP message, is combined with the information gathered in stage two to estimate the position with very high accuracy. As the location of the luminaires is approximately known, the computational complexity of the image processing is significantly reduced.

We use photogrammetry to determine the position of the receiver. After the LED beacons have been identified and the BIP messages, stating the position of the reference points within a local (or global) coordinate system, have been decoded in stage one, the reference points are located in the image plane and, finally, a triangulation algorithm is used.

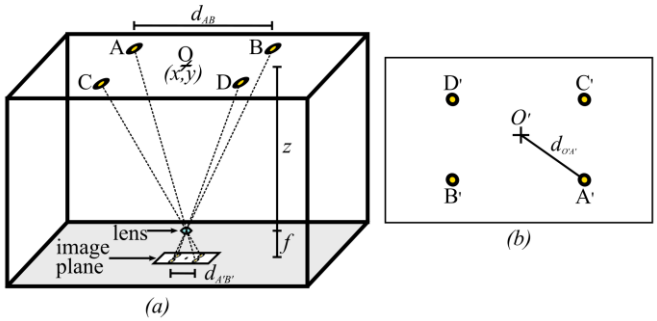

Fig. 5. (a) Room with image of ceiling captured and (b) image plane

In Fig. 5, the camera has captured an image of the ceiling showing four LED beacons. In Fig. 5 (a), the focal length of the camera, f, is a known value. The distance between the LEDs, A and B, can be easily determined in both the image and room coordinates. To determine the position in the room, first we must determine the height, z, using the ratio of the distance between two beacons: $z : f = d_{AB} : d_{A'B'}$. From this relationship, we obtain

$$\hat{z} = f \frac{\sqrt{\left(x_A - x_B\right)^2 + \left(y_A - y_B\right)^2}}{\sqrt{\left(x_{A'} - x_{B'}\right)^2 + \left(y_{A'} - y_{B'}\right)^2}} \tag{10}$$

We then repeat the calculation in (10) for all possible combinations of LED beacons and use the mean of these values to estimate the height. Once the height is known, we calculate an estimate for $\hat{x}$ and $\hat{y}$, using

$$\frac{z}{f} = \frac{d_{OA}}{d_{O'A'}} = \frac{d_{OB}}{d_{O'B'}} = \frac{d_{OC}}{d_{O'C'}} = \frac{d_{OD}}{d_{O'D'}} \tag{11}$$

The distance from the origin in the image plane, O', to each beacon, shown in Fig. 5 (b), can be determined using image processing, whilst the corresponding origin in room coordinates, O, is the (x, y) location of the receiver. From (11), we get

$$\begin{aligned}\left(d_{OA}^2 - d_{OB}^2 - x_A^2 + x_B^2 - y_A^2 + y_B^2\right)/2 &= x(x_B - x_A) + y(y_B - y_A)\\ \left(d_{OB}^2 - d_{OC}^2 - x_B^2 + x_C^2 - y_B^2 + y_C^2\right)/2 &= x(x_C - x_B) + y(y_C - y_B)\\ \left(d_{OC}^2 - d_{OD}^2 - x_C^2 + x_D^2 - y_C^2 + y_D^2\right)/2 &= x(x_D - x_C) + y(y_D - y_C)\end{aligned} \quad (12)$$

This overdetermined set of equations can easily be solved using linear least squares regression. In reality, the receiver may be tilted at arbitrary angles and thus additional algorithms are needed to compensate for these rotations.

C. Reference Points

In this section, we describe the use of visible reference points. The use of these in conjunction with the new two-stage receiver has two major advantages – it makes the new receiver more accurate and it makes it compatible with any shape of luminaire. In this paper we use the term 'reference points', these play a similar role to anchor nodes or landmarks in other positioning systems.

In principle, reference points can be any specific position within the luminaire as long as they can be unambiguously identified from the image taken in the second stage. For example, a reference point could be a given corner of the luminaire or a single colored LED. The form of the reference point can either be defined for the entire system or, can be transmitted as part of the BIP message. For example, a system could be built where every positioning luminaire has one red LED which is the reference point for that luminaire, or a more versatile system could be built where the BIP messages convey both the type and position of the reference point in each luminaire.

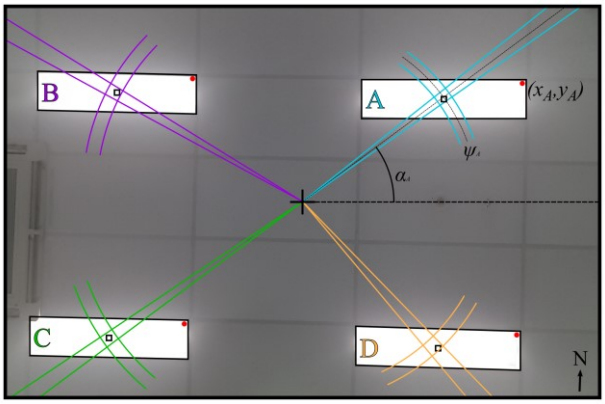

Fig. 6. Example image captured by smartphone camera with overlay showing the information provided by stage one.

Fig. 6 shows a practical example of the use of reference points. It shows an image of a ceiling on which there are four separate batten luminaires. It was captured using a front-facing smartphone camera. Batten luminaires are often used in commercial and industrial settings and consist of many LEDs in a linear array. In our new system some, or all, of the LEDs can be used to transmit positioning information. In this example, we assume a LED in the center of each luminaire is used as the beacon LED. The overlay demonstrates how the incident and polar angle estimates, from stage one, are used to locate the LED beacons and, by extension, the luminaires, in the image plane. For example, the LED beacon in luminaire A is estimated to have an incident angle of ψ_1 and a polar angle of α_1. The colored lines represent the uncertainty in the estimation and thus the area bounded by the blue lines should contain the LED beacon. This information is then matched with the BIP message that was decoded by the QADA. So now the second stage knows from the BIP the precise position of the reference point in each luminaire and its position on the image, shown as a red dot. These values are then used in (11) to calculate the receiver position.

Although we do not analyze it in detail in this paper, the concept of reference points can be extended to the use of multiple reference points within one luminaire. This would be particularly useful for large area luminaires such as the batten luminaire as fewer LED beacons are required to support triangulation.

III. Simulation Results

In this section, we investigate the performance of the QADA as the position of the receiver and the height of the ceiling is varied. We start with a room with dimensions $3\,\text{m} \times 3\,\text{m} \times 2.4\,\text{m}$ and a single LED installed in the center of the ceiling, shown in Fig. 7.

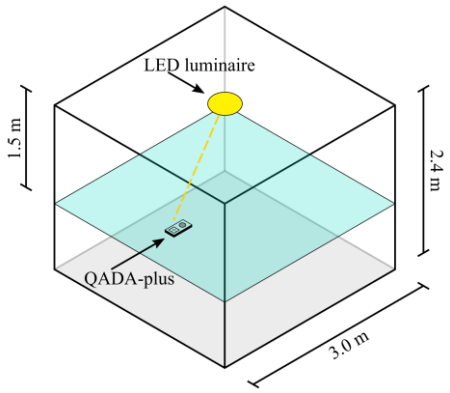

Fig. 7. Schematic of the room with dimensions 3 m x 3 m x 2.4 m that is used in the initial simulation. A single LED is located at the center of the ceiling.

We first assume that the receiver is located at a vertical distance of 1.5 m from the ceiling and that the optical power of the LED beacon is 3 W. For simplicity, we model the LED beacon as a point source. The transmitted signal is sampled at the Nyquist rate and the samples are averaged over 0.01 seconds. This allows for rapid position updates. The rest of the simulation parameters can be found in Table 1.

TABLE 1. Simulation Parameters

Parameter	Value
Quadrant PD size	5 mm × 5 mm
Aperture height	2.5 mm
Responsivity	0.25 A/W
Electrical bandwidth	1 MHz
Optical bandwidth	300 nm
Noise Equivalent Power	1.9×10^{-14} W/$\sqrt{\text{Hz}}$
Spectral irradiance	6.2×10^{-6} W/$\left(\text{nm.cm}^2\right)$

A. *Angular Diversity of QADA*

First, we analyze the angular diversity of the QADA receiver. In Fig. 8, the channel gains of the QADA receiver are presented for all possible receiver positions using the indoor scenario described in Fig. 7. Each subplot in Fig. 8 shows the channel gains between the LED beacon and a single quadrant as a function of the QADA receiver's position. We can see that, when the QADA receiver is located in the center of the room, the channel gains of the four quadrants are relatively large, but have very similar values. However, when the QADA receiver is located close to the corner of the room, the similarity between these four channel gains is significantly reduced. An important feature is that the relationship between these four channel gains is different at every point so the gains, and consequently the photocurrents, uniquely determine the position.

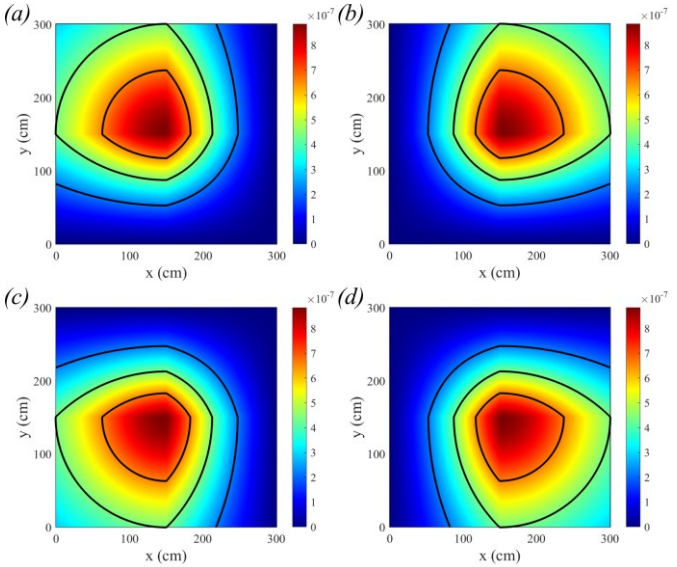

Fig. 8. Channel gain plot for all positions in the room. Each plot represents the channel gain for a single quadrant of the PD.

B. *AOA estimation*

We now investigate how the accuracy of AOA estimation varies as a function of receiver position. Fig. 9 shows the rMSE and the absolute error in AOA estimation. In Fig. 9 (a) it can be seen that the absolute errors in the estimation of the incident angle are very small for all positions; the largest absolute error in incident angle estimation is only 8.2×10^{-4} degrees. In the corners, where the incident angles are largest, the performance is worst. This is due to the low signal power resulting from lower area of overlap of the light spot and the dependence on d^{-2} and $\cos(\psi)^2$, as expressed in (4). In Fig. 9 (b), it can be seen that the absolute errors in polar angle estimation are also very small for the majority of positions, with most errors below 1×10^{-3} degrees. This is similar in magnitude to the errors in Fig. 9 (a). The largest absolute error in estimation for the polar angle is 0.0117 degrees which is directly below the luminaire. This is because small errors in the estimation of $x_1(t)$ and

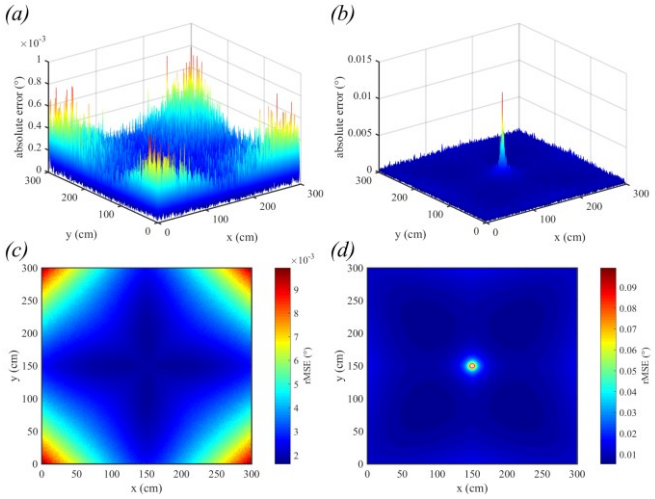

Fig. 9. Absolute error in (a) incident angle and (b) polar angle estimation. rMSE for (c) incident angle and (d) polar angle. For all plots, the receiver is 150 cm below the ceiling and the transmitted power is 3 W.

$y_1(t)$ in these positions can result in large errors in the polar angle estimation.

In Fig. 9 (c) and (d) we look at the root mean square error (rMSE) for incident and polar angle estimation. In general, the rMSE are very small for all positions, but in both plots, we can see that the error is greater at the extremities, as expected. Also, for the polar angle, the central values are also high as we saw in Fig. 9 (b). For clarity, the center values in Fig. 9 (d) have been truncated and thus, the true maximum value was 0.2892°. This is still a very small value. Additionally, the rMSE for the polar angle is smallest when closest to $45°\pm90n°$, where n is any integer. We can extrapolate this data to any LED in any position in the room as it encompasses the entire FOV of the QADA.

To investigate how sensitive the performance of the QADA is to variation in the parameters, we now change the vertical height to 3 m and the transmitted optical power to 1 W. This causes a significant reduction in received optical power. The results are shown in Fig. 10. The overall trends are very similar, however, the magnitude of the absolute error and rMSE are greater. In Fig. 10 (a) we can see that the absolute error for incident angle in the center is worse and in Fig. 10 (b) that a larger portion of the center has a relatively large error than in Fig. 9 (b).

In Fig. 10 (c) and (d) we again look at the rMSE for incident and polar angle estimation. It is important to note that because the height of the room has been increased, the range of incident angles represented is smaller. The rMSE for incident angle are again very small, whilst the rMSE for polar angles have increased but are still small. Again, we have cropped the central values for clarity. It can be seen that the circle of cropped values in the center is larger than Fig. 9 (d). The QADA has difficulty estimating angles when it is directly below the luminaire and these difficulties become more evident as the SNR decreases. The similarities in channel gain for all four quadrants, and hence the lack of angular diversity, at these positions, is a reason for this limitation.

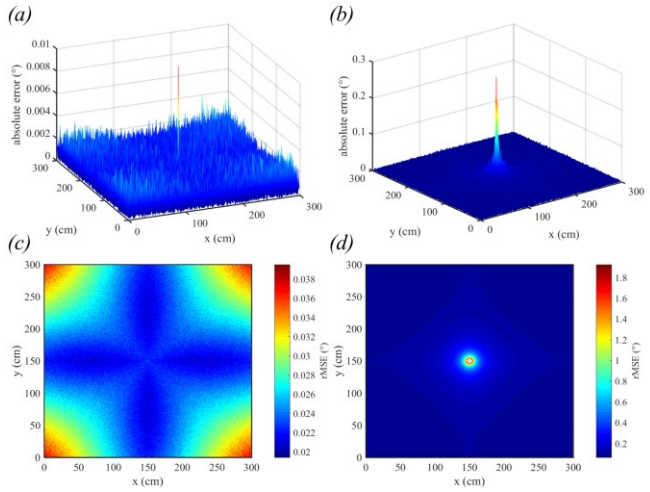

Fig. 10. Absolute error in (a) incident angle and (b) polar angle estimation. rMSE for (c) incident angle and (d) polar angle. For all plots, the receiver is 300 cm below the ceiling and the transmitted power is 1 W

C. Impact of varying height

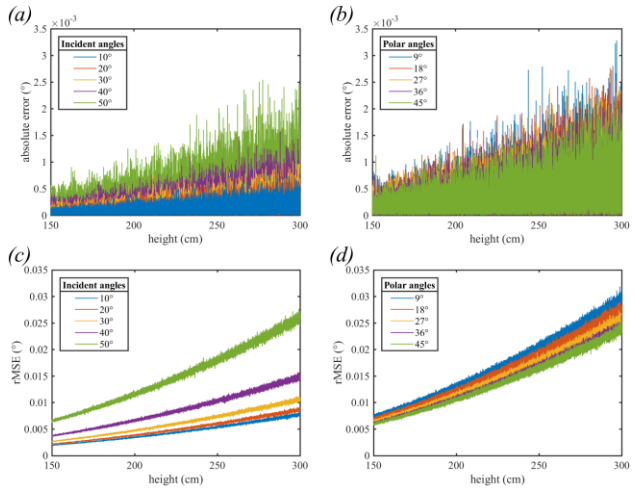

Fig. 11. Absolute error in (a) incident angle and (b) polar angle estimation and rMSE for (c) incident angle and (d) polar angle. Height is varying from 150 cm to 300 cm

We further analyze the impact of increasing the vertical distance, h, between the transmitter and receiver. In Fig. 11, for all angles and heights, the absolute errors and rMSE are small. In Fig. 11 (a) and (c) we keep the polar angle fixed at 45° and vary the incident angle between 10° and 50°. In general, the performance degrades as the height increases for all incident angles due to the reduced optical power received. Larger incident angles are impacted more than smaller incident angles due to the lower SNR.

The rMSE and error in polar angle estimation are shown in Fig. 11 (b) and (d). The incident angle is fixed at 25° and we show polar angles in the first 45° only. These can be extrapolated to other polar angles because of the repeating pattern visible in Fig. 9 (d). The estimation of polar angle is impacted in a similar way to the estimation of incident angle with the worst performance occurring at the largest distance between transmitter and receiver. Also, consistent with Fig. 9, the polar angle 45°performs best.

D. Impact of varying power

We now vary the transmitted power and fix the height at 1.5 m. The power received by QADA is directly proportional to the power transmitted by the LED beacon. The results are shown in Fig. 12. As transmitted power increases, the performance improves, as we expect. The general trends are very similar to the previous example with the varying vertical height, albeit inverted. Interestingly, there is a rapid improvement in performance between 0.5 W and 1 W, with diminishing returns thereafter.

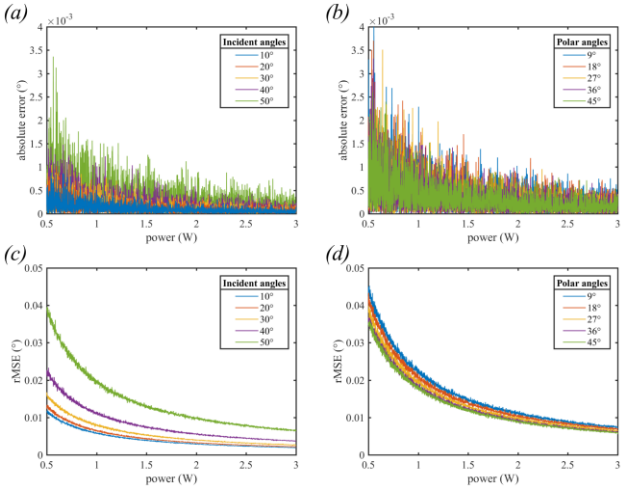

Fig. 12. Absolute error in (a) incident angle and (b) polar angle estimation and rMSE for (c) incident angle and (d) polar angle. Power is varying from 0.5 W to 1 W.

IV. Discussion

The important advantage of this new two-stage hybrid system is that it exploits the strengths of each individual method. In the previous section, it was shown that in ideal circumstances the QADA alone gives excellent estimates of angle of arrival, however, in practice, many factors may degrade the performance, including dust on the aperture, very high ceilings, dimmed luminaires or manufacturing imperfections. By moving to a two-stage system, we relax the requirements for accuracy in the QADA and create a system that is likely to be very robust in most or all realistic applications. The use of visible reference points enables the new two-stage receiver to be used for any shape of luminaire.

The performance of the second, image-based, stage depends very much on the specifications of the camera. As an example, we consider the front-facing camera of a current flagship smartphone. Current flagship smartphones have front cameras with resolution in the range of 7-8 MP, a maximum frame rate of 30 fps, and a wide FOV. Although the back cameras traditionally have higher resolution, it is likely that it will be the front camera that has the luminaires within its FOV, as the user will typically be looking at the screen. If we assume a maximum indoor movement speed of 10 km/hr, which equates to 2.78 m/s, and also assume that images are captured

every 0.033 seconds (30 fps), then the position will have only changed by a maximum of 9 cm between estimates. In most indoor applications the receiver position will change much more slowly or even be stationary for long periods of time. So, the accuracy and speed of the new system is likely to be more than adequate for the majority of future applications.

This completely new receiver design opens up many important areas for future study. Questions to be answered include: How can image processing algorithms be optimized for use in the QADA-plus receiver, and what accuracy can they achieve? How does the accuracy depend on the position of the LED beacon within the luminaire? What is the optimum type and position of visible reference point? And can multiple reference points within one luminaire improve performance?

V. Conclusion

In this paper, we have introduced a new two-stage receiver structure for visible light positioning. The new structure uses two sensors, one of which is a PD-based sensor and the other is an image-based sensor. We describe how this combination exploits both the ability of PDs to receive and demodulate high frequency signals and the ability of image-based sensors to provide very accurate positioning information. The paper also introduces the use of visible reference points in VLP. These are highly localized features which can be readily identified within an image. Potential reference points are a single colored LED within the luminaire, or a specific corner of the luminaire. The use of precise reference points allows very accurate positioning even when the LED beacons are distributed rather than point sources. Extensive simulation results are presented for the case where the PD-based sensor is a QADA. We have shown that, for a range of practical scenarios, the QADA has excellent angular diversity and can provide very accurate AOA estimation. For the case of a high ceiling and low transmitted power, the majority of errors in estimation of incident and polar angle were below 0.003° and 0.02°, respectively. The QADA sensor has the very important practical advantage over other angular diversity receivers that it has compact planar structure. This advantage is shared by the QADA-plus which is the new two-stage structure where a QADA is used in the first stage.

References

[1] J. Armstrong, Y. A. Sekercioglu, and A. Neild, "Visible light positioning: a roadmap for international standardization," *IEEE Commun. Mag.*, vol. 51, no. 12, pp. 68–73, Dec. 2013.

[2] J. Luo, L. Fan, and H. Li, "Indoor Positioning Systems Based on Visible Light Communication: State of the Art," *IEEE Commun. Surv. Tutor.*, vol. 19, no. 4, pp. 2871–2893, Fourthquarter 2017.

[3] H. Liu, H. Darabi, P. Banerjee, and J. Liu, "Survey of Wireless Indoor Positioning Techniques and Systems," *IEEE Trans. Syst. Man Cybern. Part C Appl. Rev.*, vol. 37, no. 6, pp. 1067–1080, Nov. 2007.

[4] H. Zheng, Z. Xu, C. Yu, and M. Gurusamy, "A 3-D high accuracy positioning system based on visible light communication with novel positioning algorithm," *Opt. Commun.*, vol. 396, no. Supplement C, pp. 160–168, Aug. 2017.

[5] W. Gu, M. Aminikashani, P. Deng, and M. Kavehrad, "Impact of Multipath Reflections on the Performance of Indoor Visible Light Positioning Systems," *J. Light. Technol.*, vol. 34, no. 10, pp. 2578–2587, May 2016.

[6] H. Steendam, T. Q. Wang, and J. Armstrong, "Theoretical Lower Bound for Indoor Visible Light Positioning Using Received Signal Strength Measurements and an Aperture-Based Receiver," *J. Light. Technol.*, vol. 35, no. 2, pp. 309-319, Jan 2017.

[7] T. Q. Wang, Y. A. Sekercioglu, A. Neild, and J. Armstrong, "Position Accuracy of Time-of-Arrival Based Ranging Using Visible Light With Application in Indoor Localization Systems," *J. Light. Technol.*, vol. 31, no. 20, pp. 3302–3308, Oct. 2013.

[8] T.-H. Do and M. Yoo, "TDOA-based indoor positioning using visible light," *Photonic Netw. Commun.*, vol. 27, no. 2, pp. 80–88, Apr. 2014.

[9] J. Y. Kim, S. H. Yang, Y. H. Son, and S. K. Han, "High-resolution indoor positioning using light emitting diode visible light and camera image sensor," *IET Optoelectron.*, vol. 10, no. 5, pp. 184–192, 2016.

[10] M. H. Bergen, X. Jin, D. Guerrero, H. A. L. F. Chaves, N. V. Fredeen, and J. F. Holzman, "Design and Implementation of an Optical Receiver for Angle-of-Arrival-Based Positioning," *J. Light. Technol.*, vol. 35, no. 18, pp. 3877–3885, Sep. 2017.

[11] Y.-S. Kuo, P. Pannuto, K.-J. Hsiao, and P. Dutta, "Luxapose: indoor positioning with mobile phones and visible light," in *Proceedings of the Annual International Conference on Mobile Computing and Networking, MOBICOM*, Maui; United States, 2014, pp. 447–458.

[12] S. H. Yang, H. S. Kim, Y. H. Son, and S. K. Han, "Three-Dimensional Visible Light Indoor Localization Using AOA and RSS With Multiple Optical Receivers," *J. Light. Technol.*, vol. 32, no. 14, pp. 2480–2485, Jul. 2014.

[13] L. Wei, H. Zhang, B. Yu, J. Song, and Y. Guan, "Cubic-Receiver-Based Indoor Optical Wireless Location System," *IEEE Photonics J.*, vol. 8, no. 1, pp. 1–7, Feb. 2016.

[14] H. Steendam, "A 3D Positioning Algorithm for AOA-Based VLP with an Aperture-Based Receiver," *IEEE J. Sel. Areas Commun.*, vol. 36, no. 1, pp. 23–33, Jan. 2018.

[15] A. Arafa, S. Dalmiya, R. Klukas, and J. F. Holzman, "Angle-of-arrival reception for optical wireless location technology," *Opt. Express*, vol. 23, no. 6, pp. 7755–7766, Mar. 2015.

[16] "IEEE Recommended Practices for Modulating Current in High-Brightness LEDs for Mitigating Health Risks to Viewers," *IEEE Std 1789-2015*, pp. 1–80, Jun. 2015.

[17] R. Zhang, W. D. Zhong, Q. Kemao, and S. Zhang, "A Single LED Positioning System Based on Circle Projection," *IEEE Photonics J.*, vol. 9, no. 4, pp. 1–9, Aug. 2017.

[18] S. Cincotta, C. He, A. Neild, and J. Armstrong, "High angular resolution visible light positioning using a quadrant photodiode angular diversity aperture receiver (QADA)," *Opt. Express*, vol. 26, no. 7, pp. 9230–9242, Apr. 2018.

[19] S. Cincotta, A. Neild, C. He, and J. Armstrong, "Visible Light Positioning Using an Aperture and a Quadrant Photodiode," in *2017 IEEE Globecom Workshops (GC Wkshps)*, 2017, pp. 1–6.

[20] A. M. Nugrowati, W. G. Stam, and J. P. Woerdman, "Position measurement of non-integer OAM beams with structurally invariant propagation," *Opt. Express*, vol. 20, no. 25, pp. 27429–27441, Dec. 2012.

[21] J. H. G. Huisstede, K. O. van der Werf, M. L. Bennink, and V. Subramaniam, "Force detection in optical tweezers using backscattered light," *Opt. Express*, vol. 13, no. 4, pp. 1113–1123, Feb. 2005.

[22] J. M. Kahn and J. R. Barry, "Wireless infrared communications," *Proc. IEEE*, vol. 85, no. 2, pp. 265–298, Feb. 1997.

[23] J. Proakis, M. Salehi, and G. Bauch, *Contemporary Communication Systems using MATLAB*, 3rd edition. Stamford, USA: Cengage Learning, 2013.

[24] P. Huynh and M. Yoo, "VLC-Based Positioning System for an Indoor Environment Using an Image Sensor and an Accelerometer Sensor," *Sensors*, vol. 16, no. 6, p. 783, May 2016.

[25] R. Zhang, W. D. Zhong, K. Qian, and D. Wu, "Image Sensor Based Visible Light Positioning System With Improved Positioning Algorithm," *IEEE Access*, vol. 5, pp. 6087–6094, 2017.

[26] M. H. Bergen *et al.*, "Design and optimization of indoor optical wireless positioning systems," in *Photonic Instrumentation Engineering III*, 2016, vol. 9754, p. 97540A.

[27] C. Danakis, M. Afgani, G. Povey, I. Underwood, and H. Haas, "Using a CMOS camera sensor for visible light communication," in *2012 IEEE Globecom Workshops*, 2012, pp. 1244–1248.

[28] Y. Nakazawa, H. Makino, K. Nishimori, D. Wakatsuki, and H. Komagata, "Indoor positioning using a high-speed, fish-eye lens-equipped camera in Visible Light Communication," in *International Conference on Indoor Positioning and Indoor Navigation*, 2013, pp. 1–8.